

Effect of magnetic flux advection on the dynamics of shock in accretion flow around a rotating black hole

Biplob Sarkar^{1,3} and Anjali Rao²

¹ Faculty of Science & Technology, The ICFAI University Tripura, Agartala, 799210, India;
biplobsarkar@iutripura.edu.in, meetbiplob@yahoo.com

² Department of Physics and Astronomy, University of Southampton, Highfield, Southampton SO17 1BJ, UK

³ Department of Applied Sciences, Tezpur University, Napaam-784028, Tezpur, Assam, India

Received 2019 May 8; accepted 2019 October 14

Abstract We investigate the dynamical behavior of a magnetized, dissipative accretion flow around a rapidly rotating black hole. We solve the magnetohydrodynamic equations and calculate the transonic accretion solutions which may contain discontinuous shock transitions. We investigate the effect of ζ -parameter (parametrizing the radial variation of the toroidal magnetic flux advection rate) on the dynamical behavior of shocks. For a rapidly rotating black hole and for fixed injection parameters at the outer edge, we show that stationary shocks are sustained in the global magnetized accretion solutions for a wide range of ζ and accretion rate (\dot{m}). To investigate the observational implications, we consider dissipative shocks and estimate the maximum accessible energy from the post-shock corona (PSC) for nine stellar mass black hole candidates. We compare this with the observed radio jet kinetic power reported in the literature, whenever available. We find close agreement between the estimated values from our model and those reported in the literature.

Key words: accretion, accretion discs — magnetohydrodynamics — stars: black holes — shock waves — ISM: jets and outflows

1 INTRODUCTION

Magnetic fields have a significant effect in a variety of astrophysical processes. Specifically in an accretion disc, there must be transport of angular momentum outwards so that matter can fall in at the central object. In this process, the utility of magnetic fields in the accretion disc was first discussed by Shakura & Sunyaev (1973). By considering the magnetic field to be turbulent, the authors integrated its role with the viscosity in the accretion disc which is well-known as the α -parameter these days. Moreover, magnetic fields play a significant role in the origin of a bi-directional jet from the inner region of the accretion disc around a black hole (BH). Blandford & Znajek (1977) proposed that a relativistic jet may be powered by the rotational energy of the BH via torque exerted by magnetic field lines threading the BH horizon. In an alternative mechanism, Blandford & Payne (1982) suggested that a spinning BH actually causes the ordered magnetic field in the accretion disc to corotate with the accreting matter and this drives quasi-relativistic jets via the release of gravitational potential energy. Again, it was shown by Balbus

& Hawley (1991) that the Magneto-Rotational Instability (MRI) may give rise to the disc viscosity, where even a weak magnetic field can make the accretion flow go turbulent, leading to the outward transport of angular momentum. Recent three-dimensional (3D) magnetohydrodynamic (MHD) simulations assuming azimuthal magnetic fields have further demonstrated the formation of a magnetically supported accretion disc around a BH (Machida et al. 2006; Johansen & Levin 2008). An optically thin accretion disc supported by magnetic pressure can account for the “Bright/Hard” state in BH candidates (BHCs) which is observed when the accretion disc undergoes transition from the Low/Hard state to the High/Soft state (Oda et al. 2010, 2012).

In the model of magnetized accretion flow around BHs considered by Oda et al. (2007, 2012); Sarkar & Das (2016); Das & Sarkar (2018), the parameter ζ parametrizes the radial variation of the toroidal magnetic flux advection rate ($\dot{\Phi}$). Oda et al. (2012) demonstrated that the change in ζ results in modification of $\dot{\Phi}$ which is responsible for the state transitions in BHCs. When $\dot{\Phi}$ is relatively high and \dot{M} surpasses a critical limit for the trigger of cooling in-

stability, an advection dominated accretion flow (ADAF) (Ichimaru 1977; Narayan & Yi 1994, 1995; Abramowicz et al. 1995) develops towards a magnetic pressure dominated disc. In this situation, Oda et al. (2012) proposed that the transition of the accretion disc would be bright hard-to-soft. While for a low $\dot{\Phi}$, when \dot{M} surpasses the limit, the ADAF advances towards an optically thick disc. In this situation, Oda et al. (2012) suggested that the transition would be dark hard-to-soft, which happens at under $0.1 L_{\text{Edd}}$ (Oda et al. 2010).

Another significant aspect in the study of accretion flow around a BH is the existence of global accretion solutions containing a shock, which have a special importance. Such shocked accretion solutions occur when the supersonic accretion flow approaching a BH experiences the centrifugal barrier in the vicinity of the BH. Due to the centrifugal repulsion, the supersonic flow may undergo a shock transition to become subsonic and the post-shock corona (hereafter PSC) (Aktar et al. 2015; Sarkar & Das 2016; Dihingia et al. 2019) becomes hot, dense and puffed up (Fukue 1987; Lu & Yuan 1998; Das et al. 2001; Gu & Lu 2004; Das & Choi 2009; Chattopadhyay & Chakrabarti 2011; Sarkar & Das 2018; Dihingia et al. 2018b). Shocked accretion solutions around BHs have the potential to explain many intriguing features of BHCs like the origin of outflows, jets (Das et al. 2014a,b, and references therein) and quasi-periodic oscillations (QPOs) in the hard X-ray spectra of BHCs (Molteni et al. 1996; Chakrabarti et al. 2004).

In recent years, Sarkar & Das (2015, 2016); Sarkar et al. (2018); Sarkar & Das (2018) have extensively investigated the implication of shocks in accretion flows around non-rotating BHs, where the disc is threaded by toroidal magnetic fields. Das & Sarkar (2018) extended the study to investigate the combined effect of viscosity and toroidal magnetic fields on the dynamical structure of the global accretion flow around rotating BHs. In these works, the authors assumed $\zeta = 1$ throughout, as a representative case. However, in general it is expected that the variation of ζ will have a significant effect on the radial structure of the disc. In particular, Oda et al. (2007) showed that the variation of ζ affects the temperature, plasma- β , accretion rate and optical depth in the disc. Since ζ will affect the angular momentum transport in the disc as well, the dynamics of a shock are also likely to be governed by the value of ζ . In this paper, we aim to investigate the effect of ζ on the dynamical behavior of shocks in a viscous axisymmetric magnetized accretion flow around a rapidly spinning BH. To mimic the space-time geometry around a spinning BH, we use the pseudo Kerr potential introduced by Chakrabarti & Mondal (2006). The adopted pseudo potential in this work represents a rotating BH with spin parameter $a_s \lesssim 0.8$. The relevant works re-

lated to other forms of pseudo-potentials commonly used by researchers are Chakrabarti & Khanna (1992); Løvås (1998); Artemova et al. (1996); Semerák & Karas (1999); Mukhopadhyay (2002); Ivanov & Prodanov (2005); Ghosh & Mukhopadhyay (2007); Ghosh et al. (2014); Karas & Abramowicz (2014). Very recently, Dihingia et al. (2018a), suggested another effective pseudo-potential which exactly describes the space-time geometry around a Kerr BH for the range of spin $0 \leq a_s < 1$. The focus of the present work is to determine the critical value of ζ which would sustain standing shocks in the magnetized accretion solutions around a rapidly rotating BH. Also, we demonstrate that a wide range of ζ sustains standing shocks in the accretion flow. Further for fixed flow parameters at the outer edge, we show that for a flow with higher ζ , the critical accretion rate (\dot{m}^{cri}) that sustains a shock is lower. Finally, we employ the present formalism to calculate the maximum shock luminosity ($\mathcal{L}_{\text{shock}}^{\text{max}}$) that corresponds to the maximum energy dissipated across the shock. This is done for nine stellar mass BH sources, where the mass, accretion rate and spin of the individual sources are taken from the literature. We compare $\mathcal{L}_{\text{shock}}^{\text{max}}$ with the reported values of jet kinetic power of the sources in the literature, whenever available, and we find close agreement between the two.

In the following, we first present the model assumptions and governing equations and the methodology to solve them (Sect. 2). In Section 3, we present the shocked global accretion solutions, the properties of shock and the critical values of ζ^{cri} and \dot{m}^{cri} for shock. Next, in Section 4, we compute the maximum shock luminosity from our model and compare it for several stellar mass BH sources. Finally, we present the summary of the work in Section 5.

2 MODEL FOR THE ACCRETION FLOW

The structure of magnetic fields in the accretion disc is considered to be the same as described in Oda et al. (2012). On the basis of the results obtained from 3D global as well as local MHD simulations of accretion flow around BHs, we consider the magnetic fields in the accretion disc to be turbulent and dominated by the toroidal component (Hirose et al. 2006; Machida et al. 2006; Johansen & Levin 2008). According to the results of these simulations, the magnetic fields in the disc are decomposed into the mean fields, denoted by $\mathbf{B} = (0, \langle B_\phi \rangle, 0)$, and the fluctuating fields, $\delta\mathbf{B} = (\delta B_r, \delta B_\phi, \delta B_z)$. Here, ‘ $\langle \rangle$ ’ expresses the azimuthal average of any quantity. The fluctuating components of magnetic fields disappear on azimuthally averaging ($\langle \delta\mathbf{B} \rangle = 0$). Moreover, the azimuthal component of the magnetic field is much more significant as compared to the radial and vertical components, $|\langle B_\phi \rangle + \delta B_\phi| \gg |\delta B_r|$ and $|\delta B_z|$ (see fig. 2 of Oda et al. (2012)). Eventually, the azimuthally averaged form

of the magnetic field is obtained as $\langle \mathbf{B} \rangle = \langle B_\phi \rangle \hat{\phi}$ (Oda et al. 2007).

2.1 Governing Equations

In this work, we consider a steady, thin and axisymmetric magnetized accretion flow around a rotating BH. Throughout the paper, we express the radial coordinate (x) in units of $r_g = GM_{\text{BH}}/c^2$, where G is the universal gravitational constant, M_{BH} is the mass of the BH and c is the speed of light. Also, flow velocity is measured in units of c and time is measured in units of GM_{BH}/c^3 . We assume the (x, ϕ, z) coordinate system where the accretion flow is confined in the $x - \phi$ plane and the BH is located at the center of the coordinate system.

We denote the dynamical flow variables, namely, radial velocity, sound speed, mass density, specific angular momentum, temperature, adiabatic index, specific entropy, gas pressure and magnetic pressure of the flow by the symbols $u, c_s, \rho, \lambda, T, \gamma, s, p_{\text{gas}}$ and p_{mag} respectively. Hence the mass flux conservation equation, radial momentum equation, azimuthal momentum equation and the entropy generation equation are, respectively,

$$\dot{M} = 2\pi u \Sigma x, \quad (1)$$

$$u \frac{du}{dx} + \frac{1}{\rho} \frac{dp_{\text{tot}}}{dx} + \frac{d\Psi_{\text{eff}}}{dx} + \frac{\langle B_\phi^2 \rangle}{4\pi x \rho} = 0, \quad (2)$$

$$u \Sigma x \frac{d\lambda}{dx} + \frac{d}{dx} (x^2 \mathbb{T}_{x\phi}) = 0, \quad (3)$$

$$u T \Sigma \frac{ds}{dx} = \frac{H u}{1 - \gamma} \left(\frac{\gamma p_{\text{gas}}}{\rho} \frac{d\rho}{dx} - \frac{dp_{\text{gas}}}{dx} \right) = Q^- - Q^+. \quad (4)$$

Here, \dot{M} represents the mass accretion rate and Σ specifies the mass density of the flow averaged in the vertical direction (Matsumoto et al. 1984). It might be noticed that in the present work, we consistently regard the direction of inward radial velocity as positive. Also, p_{tot} is the total pressure of the flow which is considered to be $p_{\text{tot}} = p_{\text{gas}} + p_{\text{mag}}$. The gas pressure inside the disc is obtained as $p_{\text{gas}} = R\rho T/\mu$, where R is the gas constant and μ is the mean molecular weight. We consider $\mu = 0.5$ for a fully ionized hydrogen gas. Also, the magnetic pressure of the flow is obtained as $p_{\text{mag}} = \langle B_\phi^2 \rangle / 8\pi$. We define the magnetic parameter of the flow as $\beta = p_{\text{gas}}/p_{\text{mag}}$. Using the definition of magnetic parameter, we derive the total pressure of the flow as $p_{\text{tot}} = p_{\text{gas}}(1 + 1/\beta)$. Moreover, $\mathbb{T}_{x\phi}$ denotes the $x\phi$ component of the Maxwell stress and this component dominates the vertically integrated total stress in the flow. When velocity in the radial direction is significant in the accretion flow, $\mathbb{T}_{x\phi}$ is expressed as,

$$\mathbb{T}_{x\phi} = \frac{\langle B_x B_\phi \rangle}{4\pi} H = -\alpha_T (W + \Sigma u^2), \quad (5)$$

where H, α_T and W , respectively, denote the disc half-thickness, constant of proportionality and the vertically integrated pressure of the flow (Matsumoto et al. 1984). Along the same line as the seminal work of Shakura & Sunyaev (1973), we consider α_T to remain constant everywhere along the flow. In the event that u is insignificant, such as for a Keplerian flow, Equation (5) restores to the ‘ α -model’ (Shakura & Sunyaev 1973).

In the left-hand side of Equation (2), Ψ_{eff} is the effective potential around a spinning BH suggested by Chakrabarti & Mondal (2006). The form of Ψ_{eff} is stated as,

$$\Psi_{\text{eff}} = -\frac{\mathcal{J} + \sqrt{\mathcal{J}^2 - 4\mathcal{I}\mathcal{K}}}{2\mathcal{I}},$$

where

$$\mathcal{I} = \frac{\varepsilon^2 \lambda^2}{2x^2},$$

$$\mathcal{J} = -1 + \frac{\varepsilon^2 \varphi \lambda r^2}{x^2} + \frac{2\lambda a_s}{x r^2},$$

$$\mathcal{K} = 1 - \frac{1}{r - r_0} + \frac{2a_s \varphi}{x} + \frac{\varepsilon^2 \varphi^2 r^4}{2x^2}.$$

Here, radial distance in the cylindrical coordinates is represented by x and in spherical coordinates it is denoted by r . In addition, λ is the specific angular momentum of the flow. Further, $r_0 = 0.085a_s^2 + 0.97a_s + 0.04$, $\varphi = 2a_s/(2a_s^2 + a_s^2 x + x^3)$ and $\varepsilon^2 = (a_s^2 - 2x + x^2)/(2a_s^2/x + a_s^2 + x^2)$, where ε is the redshift factor and a_s represents the spin of the BH. The pseudo-potential applied in this work adequately describes the space-time geometry around a spinning BH for $a_s \lesssim 0.8$ (Chakrabarti & Mondal 2006).

Assuming vertical hydrostatic equilibrium, we calculate the half-thickness of the disc (H) as $H(x) = c_s \sqrt{x/(\gamma \Psi_r')}$ where $\Psi_r' = (\frac{\partial \Psi_{\text{eff}}}{\partial r})_{z < x}$, z indicates vertical scale height in the cylindrical coordinate system and $r = \sqrt{z^2 + x^2}$ (Das et al. 2010; Aktar et al. 2015). Here, the adiabatic sound speed is determined as $c_s = \sqrt{\gamma p_{\text{tot}}/\rho}$. In this work, we accept γ to remain constant throughout the flow and fix $\gamma = 4/3$ (ultra-relativistic flow) for the analysis that follows.

Equation (4) is the entropy generation equation, where the cooling rate and heating rate of the flow are represented by Q^- and Q^+ , respectively. 3D MHD simulations have revealed that the dominant process contributing to the heating of the disc is the dissipation of magnetic energy via the magnetic reconnection mechanism (Machida et al. 2006; Hirose et al. 2006; Krolik et al. 2007). In view of this, the heating rate is given by,

$$Q^+ = \frac{\langle B_x B_\phi \rangle}{4\pi} x H \frac{d\Omega}{dx} = -\alpha_T (W + \Sigma u^2) x \frac{d\Omega}{dx}, \quad (6)$$

where Ω represents the flow’s angular velocity.

Due to high temperature at the inner region of the accretion disc, it is imperative that the plasma in this region be treated as two-temperature. In such a case, the electrons in the flow can lose energy via synchrotron and bremsstrahlung emission as well as through the inverse Comptonization effects. However, in the present work, we have approximated the plasma to be single temperature. Thus, the inverse Comptonization of the electrons has been disregarded since inclusion of this process requires a two-temperature analysis. Also, due to smaller size of the accretion disc in case of stellar mass BHs, the accretion disc is strongly threaded by magnetic fields. Hence, synchrotron emission by the electrons is expected to be dominant over the bremsstrahlung process (Chattopadhyay & Chakrabarti 2002; Rajesh & Mukhopadhyay 2010). Due to the above considerations, we consider only synchrotron cooling to be active in the flow. Accordingly, the synchrotron cooling rate is written as (Shapiro & Teukolsky 1983)

$$Q^- = \frac{\tilde{S}c_s^5 \rho H}{u} \sqrt{\frac{\Psi_r'}{x^3}} \beta^2 (\beta + 1)^{-3} \quad (7)$$

with

$$\tilde{S} = 1.4827 \times 10^{18} \frac{\dot{m} \mu^2 e^4}{I_n m_e^3 \gamma^{5/2}} G^{-1} M_\odot^{-1} c^{-3},$$

where e denotes the charge of the electron and m_e represents the mass of the electron. Also, \dot{m} signifies the accretion rate in Eddington units ($\dot{M}_{\text{Edd}} = 1.39 \times 10^{17} \times M_{\text{BH}}/M_\odot \text{ g s}^{-1}$). Here, we follow Rezzolla & Zanotti (2013), Straub et al. (2014) and Yuan & Narayan (2014), and apply the efficiency factor of 1 to calculate the Eddington accretion rate. Moreover, $I_n = (2^n n!)/(2n + 1)!$ and $n (= 1/(\gamma - 1))$ indicates the polytropic index of the flow. We ignore any coupling between electron and ion and evaluate the temperature of electron in the flow using the relation $T_e = (\sqrt{m_e/m_i})T_i$ (Chattopadhyay & Chakrabarti 2002). Here, m_i indicates the mass of ion and T_i refers to the ion temperature. It can be noted that although we assume a single temperature flow, the temperature profile of ions and electrons is expected to become different at least at the inner disc region. It was indicated by Mahadevan & Quataert (1997) that the exchange of energy between ions and electrons via Coulomb collision is extremely ineffective in the accretion flow. Thus, the ions cannot attain thermal equilibrium with the electrons. The ions in principle retain the heat acquired via viscous dissipation in the disc. Again, since the relativistic electrons are much lighter than the non-relativistic ions, the electrons are able to radiate more effectively than the ions. Thus the accretion flow develops a two-temperature structure which is mostly prominent at the inner region of the disc.

Since we are dealing with hydromagnetic flows, as a consequence of induction equation in steady-state (for the

current analysis), we obtain

$$\nabla \times \left(\mathbf{u} \times \langle B_\phi \rangle \hat{\phi} - \frac{4\pi}{c} \eta \mathbf{j} \right) = 0, \quad (8)$$

where \mathbf{u} is the velocity vector, \mathbf{j} is the current density and η is the resistivity of the flow. Equation (8) is now azimuthally averaged. On account of significantly large length scales in the accretion disc, the Reynolds number achieves a very high value. As a result, we ignore the magnetic diffusivity term. Further, we also disregard the dynamo term for the present purpose. The resulting equation is then vertically integrated considering the vanishing of the azimuthally averaged toroidal magnetic fields at the surface of the disc. In view of these assumptions, the advection rate of toroidal magnetic flux is determined as

$$\dot{\Phi} = -\sqrt{4\pi} u B_0(x) H, \quad (9)$$

where,

$$\begin{aligned} B_0(x) &= \langle B_\phi \rangle (x; z = 0) \\ &= \frac{2^{5/4} \pi^{1/4} (RT)^{1/2} \Sigma^{1/2}}{\mu^{1/2} H^{1/2} \beta^{1/2}} \end{aligned}$$

represents the mean azimuthal toroidal magnetic field in the disc equatorial plane following Oda et al. (2007). In the accretion disc, it is generally expected that $\dot{\Phi}$ will vary in the radial direction due to the diffusion of magnetic fields and the dynamo action. However, to avoid the complexity of determining the magnetic diffusivity term and dynamo term self-consistently from the local variables, we follow the prescription of Oda et al. (2007) and adopt the parametric relation expressed by

$$\dot{\Phi} \left(x; \zeta, \dot{M} \right) \equiv \dot{\Phi}_{\text{inj}} \left(\frac{x}{x_{\text{inj}}} \right)^{-\zeta}, \quad (10)$$

where ζ represents a parameter describing the advection rate of magnetic flux. Further, $\dot{\Phi}_{\text{inj}}$ denotes the advection rate of the toroidal magnetic field at the injection radius (x_{inj}), or equivalently the outer edge of the accretion disc. When $\zeta = 0$, magnetic flux remains constant radially while, for $\zeta > 0$, the magnetic flux increases with the decrease of radius.

2.2 Transonic Conditions and Solution Procedure

Due to the essential transonic nature of BH accretion flows, the infalling matter is subsonic at the outer edge of the disc (x_{inj}) and enters the BH supersonically (Chakrabarti 1990). The location in the radial direction, where the flow behavior changes smoothly from subsonic state to supersonic state, is usually termed a critical point. In the following, we solve Equations (1), (2), (3), (4), (9) and (10) simultaneously in order to perform the critical point analysis (Sarkar & Das 2016, and references therein), and is given by

$$\frac{du}{dx} = \frac{\mathcal{N}}{\mathcal{D}}, \quad (11)$$

where the expressions for the numerator (\mathcal{N}) and denominator (\mathcal{D}) are provided in Das & Sarkar (2018). The expressions for the radial gradients of c_s , λ and β can also be found in Das & Sarkar (2018).

Now, the infalling matter must smoothly accrete onto the BH. This demands that the flow variables must have finite values everywhere along the flow. Thus, if the denominator \mathcal{D} in Equation (11) vanishes in any radial location, the numerator \mathcal{N} must also simultaneously vanish there ($du/dx = 0/0$), in order to maintain a smooth solution. Such a radial location is known as a critical point (x_c). This gives us two critical point conditions of $\mathcal{N} = 0$ and $\mathcal{D} = 0$. The expression of Mach number ($M = u/c_s$) at x_c is obtained by applying the condition $\mathcal{D} = 0$, which is written as

$$M_c = \sqrt{\frac{-\varkappa_2 - \sqrt{\varkappa_2^2 - 4\varkappa_1\varkappa_3}}{2\varkappa_1}}, \quad (12)$$

where

$$\varkappa_1 = 2\alpha_T^2 \gamma^2 I_n (1-\gamma)(1-2g)(\beta_c+1) - \gamma^2 [(1+\gamma)\beta_c+3],$$

$$\varkappa_2 = 2\gamma(\gamma\beta_c+2) + 4\alpha_T^2 \gamma I_n g(1-g)(1-\gamma)(\beta_c+1),$$

$$\varkappa_3 = 2\alpha_T^2 g^2 I_n (1-\gamma)(\beta_c+1),$$

where the parameter g is defined as $g = I_{n+1}/I_n$. To obtain the sound speed (c_{sc}) at x_c , we use the condition $\mathcal{N} = 0$ to get a cubic equation of the form

$$\mathcal{A}_1 c_{sc}^3 + \mathcal{A}_2 c_{sc}^2 + \mathcal{A}_3 c_{sc} + \mathcal{A}_4 = 0, \quad (13)$$

where

$$\mathcal{A}_1 = \tilde{S} \sqrt{\frac{\Psi'_r}{x_c^3}} \frac{\beta_c^2}{(\beta_c+1)^3},$$

$$\mathcal{A}_2 = \frac{2\alpha_T^2 I_n (\gamma M_c^2 + g)^2}{x_c \gamma^2} - \frac{M_c^2 (4 + 2\gamma\beta_c)}{2\gamma(1-\gamma)(\beta_c+1)} \left(\frac{d \ln \Psi'_r}{dx} \right)$$

$$- \frac{2\alpha_T^2 g I_n (\gamma M_c^2 + g)}{\gamma^2} \left(\frac{d \ln \Psi'_r}{dx} \right)$$

$$- \frac{2\{\beta_c(1+\gamma) + 3\} M_c^2}{\gamma(1-\gamma)(\beta_c+1)^2 x_c}$$

$$+ \frac{3(3 + 2\gamma\beta_c) M_c^2}{2\gamma(1-\gamma)(\beta_c+1) x_c} + \frac{6\alpha_T^2 g I_n (\gamma M_c^2 + g)}{x_c \gamma^2}$$

$$- \frac{8\alpha_T^2 g I_n (\gamma M_c^2 + g)}{\gamma^2 (\beta_c+1) x_c} - \frac{(1-4\zeta) M_c^2}{2\gamma(\beta_c+1)(1-\gamma) x_c},$$

$$\mathcal{A}_3 = - \frac{4\lambda_c \alpha_T I_n M_c (\gamma M_c^2 + g)}{x_c^2 \gamma},$$

$$\mathcal{A}_4 = \left[\frac{\{\beta_c(1+\gamma) + 3\} M_c^2}{(\gamma-1)(\beta_c+1)} - \frac{4\alpha_T^2 I_n g (\gamma M_c^2 + g)}{\gamma} \right] \times \left(\frac{d \Psi'_r}{dx} \right).$$

Here, we represent the values of the flow variables estimated at x_c with the subscript ‘c’.

Presently, we obtain the value of sound speed (c_{sc}) at x_c by supplying the accretion flow parameters in Equation (13). Then the value of u_c can be found using Equation (12). The obtained values of u_c and c_{sc} are supplied in Equation (11) to analyze the characteristics of the critical points. At x_c , du/dx possesses two particular values; one of which holds for the accretion solution and the other is for wind. If both the values of the velocity gradient at x_c are real and of reverse sign, x_c is called a ‘saddle’ type critical point (Chakrabarti 1990; Chakrabarti & Das 2004). Such a critical point is of unique significance since a global accretion solution goes through it only. In this work, since our objective is to explore the magnetized accretion flow around a BH, we consider solely the accretion solutions in the subsequent investigation.

3 RESULTS AND DISCUSSION

In order to acquire a global accretion solution, we need to derive the simultaneous solution of the coupled differential equations corresponding to the radial gradient of flow velocity (u), sound speed (c_s), angular momentum (λ) and plasma β . Additionally, the boundary values of u , c_s , λ , β and \dot{m} must be known at a given radial position (x). The Kerr parameter (a_s) and viscosity parameter (α_T) also need to be specified. It should be noted that, throughout the paper, we express angular momentum (λ) in units of the Keplerian angular momentum $\lambda_K (= \sqrt{x^3/(x-2)^2})$. Owing to the essential transonic nature of BH accretion solutions, flow must inevitably go through a critical point. Thus, it is suitable to supply the boundary flow variables at the critical point. With this, we carry out integration of the equations corresponding to the radial gradient of u , c_s , λ and β from the critical point once towards the inside up to exactly outside the BH horizon and then outward up to the outer boundary of the disc. These two sections can be joined to yield a full global transonic accretion solution. As determined by the boundary parameters, the accretion flow has to cross one critical point at the minimum and feasibly more (Sarkar & Das 2013, and references therein). A critical point which is located near the BH horizon is called an inner critical point (x_{in}) and that which is located far from the BH horizon is known as an outer critical point (x_{out}).

To begin with, we explore the effect of the ζ -parameter prescribing the magnetic flux advection rate

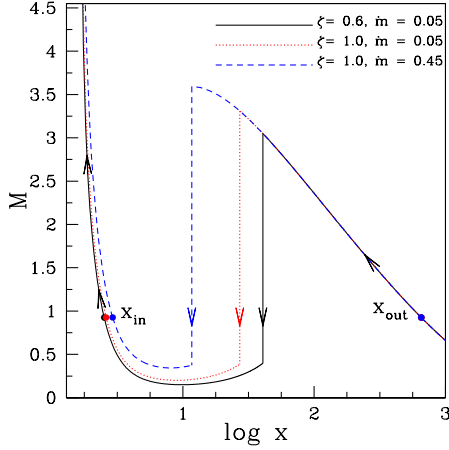


Fig. 1 Variation of Mach number as a function of logarithmic radial distance. The flows are injected from the outer edge $x_{\text{inj}} = 1000$ with specific energy $E_{\text{inj}} = 8.9 \times 10^{-4}$, angular momentum $\lambda_{\text{inj}} = 0.11014\lambda_K$, $\beta_{\text{inj}} = 10^5$ and viscosity $\alpha_T = 0.02$. The Kerr parameter is chosen as $a_s = 0.8$. Solid, dotted and dashed curves depict the results obtained for $(\zeta, \dot{m}) = (0.6, 0.05)$, $(1.0, 0.05)$ and $(1.0, 0.45)$, respectively. The vertical arrows indicate the corresponding shock transitions positioned at $x_s = 40.72$ (solid), $x_s = 27.12$ (dotted) and $x_s = 11.68$ (dashed). See text for details.

on the dynamical structure of the accretion flow that contains a shock wave. For this purpose, we fix the global parameters as $\alpha_T = 0.02$, $a_s = 0.8$ and inject matter subsonically from the outer edge of the disc at $x_{\text{inj}} = 1000$ with local flow variables as $\lambda_{\text{inj}} = 0.11014\lambda_K$, $\beta_{\text{inj}} = 10^5$ and $E_{\text{inj}} = 8.9 \times 10^{-4}$. The obtained results are depicted in Figure 1, where the variation of Mach number (M) is plotted against the logarithmic radial distance. First we inject matter with accretion rate $\dot{m} = 0.05$ and $\zeta = 0.6$. For these injection parameters, subsonic flow at the outer edge approaches the BH and becomes supersonic after crossing the outer critical point located at $x_{\text{out}} = 654.52$. The supersonic flow proceeds towards the BH and sustains a virtual centrifugally repulsive barrier in the neighborhood of the BH. Due to this obstruction, the accreting matter begins to pile up in the vicinity of the BH, leading to the increase of flow density profile. However, this accumulation of matter cannot persist indefinitely and when the density scale length achieves a critical limit, the flow may suffer a discontinuous shock transition (Frank et al. 1992). As a result of this, the ordered kinetic energy of the flow gets converted to disordered thermal energy. Whenever dynamically feasible, such a discontinuous shock jump is preferred by the laws of thermodynamics since the entropy of the flow increases after the shock (Fukue 1987; Becker & Kazanas 2001; Fukumura & Tsuruta 2004). The shock transition in a magnetized accretion flow is governed by the conservation of:

- (i) energy flux: $E_+ = E_-$,
- (ii) mass flux: $\dot{M}_+ = \dot{M}_-$,
- (iii) pressure balance: $W_+ + \Sigma_+ u_+^2 = W_- + \Sigma_- u_-^2$,
- (iv) magnetic flux advection rate: $\dot{\Phi}_+ = \dot{\Phi}_-$,

where ‘+’ and ‘-’ represent the quantities evaluated immediately after and before the shock transition (x_s) respectively (Landau & Lifshitz 1959; Sarkar & Das 2016). In the pseudo-Kerr geometry, we follow Das & Sarkar (2018) to calculate the local specific energy of the flow as $E(x) = u^2/2 + c_s^2/(\gamma - 1) + \Psi_{\text{eff}} + \langle B_\phi^2 \rangle / (4\pi\rho)$. For the present case, the shock is positioned at $x_s = 40.72$ as indicated with the solid vertical arrow. Soon after the shock transition, flow gradually gains its radial velocity due to the gravitational attraction and enters into the BH supersonically after crossing the inner critical point at $x_{\text{in}} = 2.52$. When the magnetic flux advection rate parameter is increased further as $\zeta = 1.0$ while keeping all the remaining flow parameters unaltered, we find that the shock front moves inward and settles down at $x_s = 27.12$. In the figure, this is indicated using the dotted vertical arrow. In reality, as ζ is increased, the magnetic fields carried with the accreting matter are also enhanced which raise the synchrotron cooling efficiency. Since the cooling is mostly effective at PSC, post-shock pressure reduces appreciably which eventually causes the shock front to move further towards the BH in order to preserve the pressure balance across the shock. Next, we choose $\zeta = 1.0$ and $\dot{m} = 0.45$ keeping the rest of the flow parameters the same. Due to the increase of \dot{m} , the synchrotron cooling efficiency in the flow is additionally augmented and the shock front advances further towards the horizon. The shock now forms at $x_s = 11.68$ as indicated with the dashed vertical arrow. In all the cases, arrows indicate the overall direction of flow motion towards the BH. Based on the above analysis, we consequently point out that the ζ -parameter prescribing the magnetic flux advection rate seems to play an important role in deciding the accretion disc dynamics including shock waves, in addition to accretion rate (\dot{m}).

In Figure 2, we display the radial disc structure corresponding to shock solutions considered in Figure 1. For this, we consider $M_{\text{BH}} = 10 M_\odot$ as a standard reference value. Here in each panel, we show the radial variation of a flow variable where solid, dotted and dashed curves depict results corresponding to $(\zeta = 0.6, \dot{m} = 0.05)$, $(\zeta = 1.0, \dot{m} = 0.05)$ and $(\zeta = 1.0, \dot{m} = 0.45)$, respectively. Moreover, the filled dots represent the position of the critical points. In Figure 2(a), we plot the variation of the radial velocity of the flow as a function of distance from the BH. Since the accreting matter experiences greater gravitational pull as it moves closer to the BH, the radial velocity profile steadily increases towards the horizon. Thus, the subsonic flow starting from the outer edge of the disc becomes supersonic as it crosses the outer critical point. This super-

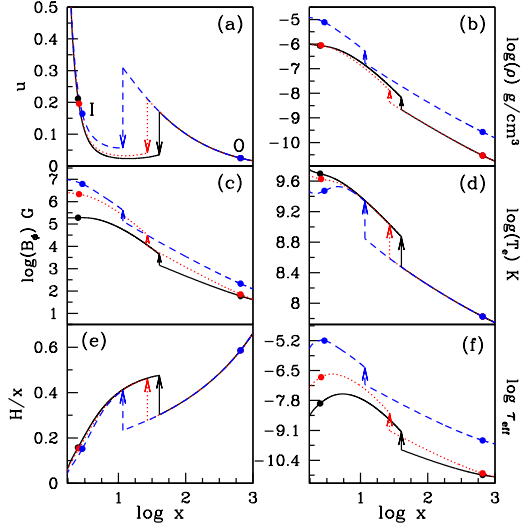


Fig. 2 Variation of (a) radial velocity, (b) density in g cm^{-3} , (c) the toroidal component of magnetic field in Gauss, (d) the electron temperature in Kelvin, (e) disc aspect ratio (H/x) and (f) effective optical depth as a function of logarithmic radial coordinate. The *solid*, *dotted* and *dashed* curves relate to the shocked accretion solutions portrayed in Figure 1. The critical points are indicated with *filled circles* where the closer one is the inner critical point and the farthest represents the outer critical point. Position of the shock is displayed using *vertical arrows*. See text for details.

sonic flow experiences centrifugal barrier in the vicinity of the BH and undergoes a shock jump to become subsonic as indicated by the downward vertical arrow in each of the three cases. The subsonic flow again becomes supersonic after passing through the inner critical point and enters the BH horizon. In Figure 2(b) we show the variation of density of the accretion flow as a function of radial distance. The density of the flow rises as the flow approaches the horizon and the density is boosted up across the shock transition. The post-shock density rises due to the reduction of flow velocity after the shock jump in order to conserve the mass flux (\dot{M}) across the shock transition. This is evident from the sudden rise in density profile in all the cases as indicated by the upward vertical arrow. Next, in Figure 2(c) we present the variation of the magnetic field strength B_ϕ as a function of radial distance. For all the cases, we find that B_ϕ steadily increases with the decrease of radial coordinate. This happens due to the increase of magnetic flux advection rate ($\dot{\Phi}$) with decreasing radius. Increase of ζ augments $\dot{\Phi}$ and leads to increase of B_ϕ profile as signified by the dotted curve. Also when \dot{m} rises, there would be an increase of magnetic field lines carried with the matter. So, the B_ϕ profile would also increase as indicated with the dashed curve. Further, B_ϕ also jumps across the shock transition due to the compression of the flow at the shock location and the conservation of $\dot{\Phi}$ across the shock. In Fig. 2(d), we show the variation of electron temperature (T_e) in

the flow as a function of radial distance. This is essential since T_e is related to the nature of the X-ray spectrum emitted from the disc. We observe a rise in T_e in the flow with decreasing radius for all the cases. T_e is catastrophically augmented across the shock jump, thereby demonstrating that the PSC is significantly hotter than the pre-shock region. When ζ value is increased from 0.6 to 1.0 (keeping \dot{m} fixed), there is increase of magnetic field strength that increases the cooling of the electrons due to synchrotron emission. Thus we observe a drop in T_e profile in the inner region (dotted curve). A further drop in the T_e profile is also observed when \dot{m} is increased to 0.45 retaining ζ fixed (dashed curve). Augmented accretion rate additionally enhances the efficiency of synchrotron emission by the electrons and also causes the drop in T_e profile. In Figure 2(e), we plot the radial variation of the aspect ratio (H/x) of the magnetized accretion disc. We find that the aspect ratio remains below unity throughout the disc for all the cases. Further, due to the high temperature and density in the PSC of the disc, the PSC becomes puffed up and a sudden rise in the disc aspect ratio is observed after the shock jump in all cases. Lastly, in Figure 2(f), we depict the radial distribution of effective optical depth in the vertical direction (τ_{eff}). In the disc, we calculate τ_{eff} using the relation $\tau_{\text{eff}} = \sqrt{\tau_{\text{syn}} \tau_{\text{es}}}$ (Rajesh & Mukhopadhyay 2010), where τ_{syn} denotes the absorption effect arising due to thermal processes and is given by $\tau_{\text{syn}} = (H \bar{q}_{\text{syn}} / 4 \bar{a} T_e^4) (GM_{\text{BH}} / c^2)$ (Rajesh & Mukhopadhyay 2010), \bar{q}_{syn} is the synchrotron emissivity (Shapiro & Teukolsky 1983) and $\bar{a} = 5.6705 \times 10^{-5} \text{ g s}^{-3} \text{ K}^{-4}$ is the Stefan-Boltzmann constant. Here, τ_{es} denotes the scattering optical depth estimated as $\tau_{\text{es}} = \kappa_{\text{es}} \rho H$ where $\kappa_{\text{es}} = 0.38 \text{ cm}^2 \text{ g}^{-1}$ is the electron scattering opacity. Here, we observe that for all the cases, τ_{eff} remains well below unity. However, a rise in τ_{eff} is observed across the shock transition in every case due to greater density at the PSC as observed in Figure 2(b). When ζ is increased retaining other parameters fixed, the magnetic activity in the disc is augmented, leading to the increase in τ_{syn} and the consequent increase of the τ_{eff} profile (dotted curve). Also, when \dot{m} rises to 0.45 keeping the rest of the parameters fixed, there is a further rise in the τ_{eff} profile due to increase of density in the accretion flow (dashed curve).

One of the pertinent aspects in understanding the magnetically supported accretion flow around the rotating BHs is to study the dependence of the shock properties on the magnetic flux advection rate ($\dot{\Phi}$). For this purpose in Figure 3, we fix the outer edge of the disc at $x_{\text{inj}} = 1000$ and inject matter to accrete with $E_{\text{inj}} = 8.9 \times 10^{-4}$, $\beta_{\text{inj}} = 10^5$, $\alpha_T = 0.02$ and $\dot{m} = 0.05$. Kerr parameter is held fixed at $a_s = 0.8$. It has already been specified that the ζ -parameter decides the advection rate of toroidal magnetic flux ($\dot{\Phi}$). Thus in Figure 3(a), we present the vari-

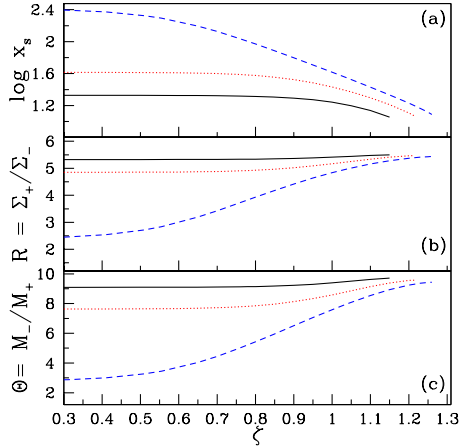


Fig. 3 Variation of (a) shock location x_s , (b) compression ratio R and (c) shock strength Θ as a function of ζ for flows injected from $x_{inj} = 1000$ with $\beta_{inj} = 10^5$, $\alpha_T = 0.02$, $E_{inj} = 8.9 \times 10^{-4}$ and $\dot{m} = 0.05$. The Kerr parameter is chosen as $a_s = 0.8$. *Solid*, *dotted* and *dashed curves* represent the results corresponding to $\lambda_{inj} = 0.10888\lambda_K$, $0.11014\lambda_K$ and $0.11141\lambda_K$ respectively. See text for details.

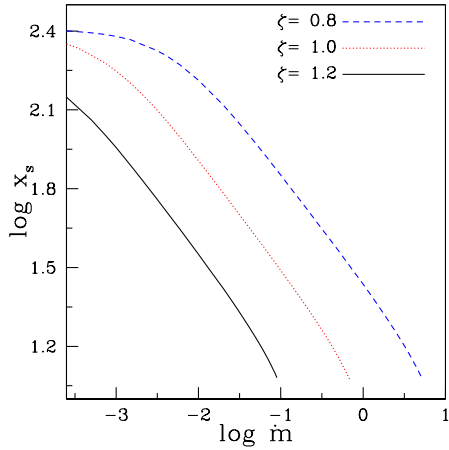


Fig. 4 Shock location (x_s) variation as a function of \dot{m} . Flow is injected from the outer edge $x_{inj} = 1000$ with $\beta_{inj} = 10^5$, $\alpha_T = 0.02$, $E_{inj} = 8.9 \times 10^{-4}$ and $\lambda_{inj} = 0.11141\lambda_K$. The spin of the BH is chosen as $a_s = 0.8$. Results plotted with *solid*, *dotted* and *dashed curves* are for $\zeta = 1.2$, 1.0 and 0.8 , respectively. See the text for details.

ation of x_s with ζ for three sets of specific angular momentum, $\lambda_{inj} = 0.10888\lambda_K$ (solid curve), $\lambda_{inj} = 0.11014\lambda_K$ (dotted curve) and $\lambda_{inj} = 0.11141\lambda_K$ (dashed curve). We observe that for a given λ_{inj} , shocks form for an ample range of ζ and when ζ is increased, the shock front moves towards the BH horizon. The increase of ζ leads to the increase of toroidal magnetic flux advection rate in the radial direction as the flow proceeds towards the BH (Oda et al. 2007, 2012). With the increase of magnetic activity in the disc, the flow gets efficiently cooled. Since the cooling efficiency is greater in the PSC due to higher temperature and density there, the post-shock pressure drops and the shock

front is pushed towards the BH in order to maintain pressure balance across it. The increase of magnetic activity in the disc also enhances the angular momentum transport towards the outer region of the disc. This weakens the centrifugal repulsion against gravity and also contributes to shift the shock towards the horizon. When ζ -parameter is increased beyond a critical value (ζ^{cri}), the shock conditions are no longer satisfied and a standing shock fails to form. Moreover, for a given ζ , we find that when flow is characterized with relatively large λ_{inj} , shocks form over a large range of distances and vice versa. This clearly indicates that shock transitions in BH accretion flows are centrifugally driven.

Now, corresponding to the shock solutions shown in Figure 3(a), we present the variation of relating shock compression ratio (R) and the shock strength (Θ) with ζ -parameter in Figure 3(b) and Figure 3(c), respectively. Here, R is defined as the ratio of the vertically integrated post-shock density to pre-shock density as $R = \Sigma_+ / \Sigma_-$. On the other hand, Θ is defined as the ratio of pre-shock to post-shock Mach number ($\Theta = M_- / M_+$). Since stronger shocks are located closer to the BH horizon, we find that R steadily increases with ζ in Figure 3(b). We ascertain that for shocks closest to the BH horizon, $R \sim 5$. Moreover, similar variational characteristics of Θ are observed in Figure 3(c) as in the case of R . It can be noticed that R and Θ are almost independent, with the flux advection rate for the results signified using solid and dotted curves respectively. The reason for this behavior is the weak angular momentum transport rate for low value of ζ . This claim is consistent with Equation (5), where $\mathbb{T}_{x\phi}$ is proportional to the sum of vertically integrated pressure of the flow (W) and the ram pressure (Σu^2). Here, W has contribution from the gas pressure (p_{gas}) as well as magnetic pressure (p_{mag}) in the flow. Now, from Figure 2(c), we find that when the ζ value is increased, the value of B_ϕ increases at a particular radial coordinate. Thus, $p_{mag} (= < B_\phi >^2 / 8\pi)$ rises with the increase of ζ for a given radial coordinate and, consequently, $\mathbb{T}_{x\phi}$ is also augmented at that location. So, ζ controls the angular momentum transport rate in the flow. The major motivation in this figure is to establish that the accretion flow admits a shock for a wide range of angular momenta as well as ζ . The chosen values of λ_{inj} for the solid and dotted curves are lower than that of the dashed curve. So for the solid and dotted curves, the shocks form closer to the BH as compared to the dashed curve. Also when ζ is low ($\lesssim 0.8$), the rate of transport of angular momentum in the disc is expected to be feeble. Due to the proximity of the shock location to the BH horizon and meager angular momentum transport rate, there is a small shift in shock location when ζ is lowered and we do not observe a significant variation in the compression ratio or shock strength for the results marked with solid and dotted curves.

In Figure 4, we show the variation of shock location (x_s) as function of \dot{m} . At the injection radius $x_{\text{inj}} = 1000$, the flow parameters are chosen as $E_{\text{inj}} = 8.9 \times 10^{-4}$, $\lambda_{\text{inj}} = 0.11141\lambda_K$, $\beta_{\text{inj}} = 10^5$ and $\alpha_T = 0.02$. The BH spin parameter is fixed as $a_s = 0.8$. Here, solid, dotted and dashed curves refer to the results corresponding to $\zeta = 1.2$, 1.0 and 0.8, respectively. We notice that for a given ζ , x_s decreases with the increase of \dot{m} . It was already pointed out that the shock front advances towards the BH when \dot{m} is increased (see Fig. 1) and the overall pressure in the PSC is expected to be reduced. Therefore, for a given ζ , we observe an anti-correlation between x_s and \dot{m} . When \dot{m} rises beyond a critical limit (\dot{m}^{cri}), standing shocks do not form since the shock conditions are not satisfied anymore. Again, x_s is also found to decrease with the increase in ζ , when \dot{m} is fixed. In reality, when the ζ parameter is augmented, synchrotron cooling efficiency in the flow is higher as there is increased magnetic activity in the disc. Due to the efficient cooling at the PSC, the post-shock pressure decreases and the shock location approaches the BH in order to maintain the pressure balance across the shock front. Thus, for a given \dot{m} , x_s anti-correlates with ζ .

4 ASTROPHYSICAL RELEVANCE

Thus far, we have dealt with non-dissipative shocks where the specific energy essentially remains conserved across the shock front (Chakrabarti 1989). However, as seen in Figure 2(f), the sudden compression of the flow at the shock causes the optical depth of the flow to rise significantly across the shock front. Since the shock is thin and the optical depth there is very high, thermal Comptonization of the photons is expected to be very important. Chakrabarti & Titarchuk (1995) pointed out that due to the thermal Comptonization process, the dissipation of energy of the accretion flow at the shock is likely. This energy dissipation mechanism eventually reduces the temperature of the flow in the PSC and the energy loss is proportional to the difference in temperature in the post- and pre-shock flows. Following this, the loss of energy (ΔE) at the shock is assessed as (Das et al. 2010)

$$\Delta E = f_d n (c_{s+}^2 - c_{s-}^2), \quad (14)$$

where c_{s-} and c_{s+} denote the pre-shock and post-shock sound speeds, respectively. Here, f_d refers to the fraction of thermal energy difference dissipated across the shock front, which is treated as a free parameter in this work (Das et al. 2010; Singh & Chakrabarti 2011; Sarkar & Das 2013; Kumar & Chattopadhyay 2013; Sarkar et al. 2018; Das & Sarkar 2018). The kinetic power lost from the disc can be evaluated by regarding the shock luminosity as in Le & Becker (2004), Le & Becker (2005), Sarkar & Das (2016) and Sarkar et al. (2018),

$$\mathcal{L}_{\text{total}} = \mathcal{L}_{\text{shock}} = \dot{M} \times \Delta E \times c^2 \text{ erg s}^{-1}, \quad (15)$$

where $\mathcal{L}_{\text{total}}$, $\mathcal{L}_{\text{shock}}$ and \dot{M} denote the kinetic power lost by the disc, the luminosity of shock and the accretion rate for a specified source, respectively. The energy loss at the shock front due to Comptonization (ΔE) is essentially a function of the number of soft photons and the number density of electrons (Mondal et al. 2014). In this paper, we fix $f_d = 0.998$ all throughout, for the sake of representation.

Subsequently, we compute the maximum luminosity of shock ($\mathcal{L}_{\text{shock}}^{\text{max}}$) relating to maximum dissipation of energy at the shock. Here, $\alpha_B = 0.001$ and $\beta_{\text{in}} = 10^5$ are considered for all cases. Also, in Oda et al. (2007), the authors have obtained radial structure of the accretion disc considering $\zeta = 1$, which remains optically thin throughout. For $\zeta \sim 0$, the authors showed that steady global transonic solutions with magnetic fields were not derived beyond a certain critical accretion rate. They further reported that for $\zeta \sim 1$, accretion solutions connecting the outer boundary to the inner region can be obtained for large accretion rates with the low- β region at the inner part of the disc. Moreover, Oda et al. (2012) stated that for small values of ζ (e.g., $\zeta \sim 0$), it is not possible to obtain the magnetically supported low- β disc solutions but the usual ADAF/radiatively inefficient accretion flow (RIAF) solutions can be explained. Further, in table 1 of Oda et al. (2012), the authors demonstrated the formation of a low- β disc can occur in global accretion solutions for $0.5 \leq \zeta \leq 1$, by suitably choosing the other disc parameters. For $\zeta > 1$, the authors additionally showed that magnetic pressure would dominate in the accretion flow even at low accretion rates. Considering all these, we argue that $\zeta \geq 0.5$ is a reasonable approximation in the accretion disc to obtain the low- β solutions and this can support the observational values. Thus, we choose $\zeta = 1$ as a representative value in the analysis that follows.

In Table 1, we present the physical parameters of the stellar mass BH sources including model parameters and compute maximum luminosity of the shock. Columns (1)–(4) of Table 1 list the names of sources, their mass (M_{BH}), accretion rate (\dot{m}) and spin (a_s). In columns (5)–(6), we provide the specific energy at the inner critical point (E_{in}) and the angular momentum at the inner critical point (λ_{in}). In column (7), we note the maximum dissipated energy ΔE^{max} and in column 8, we indicate the position of shock (x_s). In column (10), the maximum luminosity of shock $\mathcal{L}_{\text{shock}}^{\text{max}}$ is reported. Our primary objective in this examination is to estimate the upper limit of energy that can be removed from the PSC to power the outflowing matter from the disc as jets. Accordingly, we evaluate the maximum dissipated energy ΔE^{max} at the position of shock jump. For the stellar mass BH sources under consideration, we find that the evaluated luminosities of shock are in consensus with the core radio luminosity values $\mathcal{L}_{\text{jet}}^{\text{Obs}}$ (in col-

Table 1 Calculation of Luminosity of Shock

Object	M_{BH} (M_{\odot})	\dot{m} (\dot{M}_{Edd})	a_s	E_{in} (10^{-2})	λ_{in} (λ_K)	ΔE^{max} ($10^{-2}c^2$)	x_s (r_g)	$\mathcal{L}_{\text{shock}}^{\text{max}}$ (erg s^{-1})	$\mathcal{L}_{\text{jet}}^{\text{Obs}}$ (erg s^{-1})
(1)	(2)	(3)	(4)	(5)	(6)	(7)	(8)	(9)	(10)
A0620–00	6.60 ^a	5.0×10^{-4} ^b	0.12 ^c	−0.6517	0.88972	0.8754	16.54	3.61×10^{33}	1.0×10^{33} [★]
LMC X-3	6.98 ^d	2.365 ^e	0.25 ^f	−1.5036	0.85117	1.5642	16.03	3.23×10^{37}	–
H1743–322	11.21 ^g	0.127 ^h	0.4 ⁱ	−2.2296	0.76128	2.2488	15.22	4.0×10^{36}	3.60×10^{38} [★]
XTE J1550–564	9.10 ^j	0.528 ^k	0.49 ^k	−2.4323	0.68529	2.4216	14.27	1.45×10^{37}	3.41×10^{38} ^l
GRO J1655–40	5.31 ^m	0.596 ⁿ	0.7 ^o	−2.8775	0.40495	2.7427	13.25	1.08×10^{37}	1.95×10^{36} ^p
XTE J1118+480 [†]	7.50 ^q	3.0×10^{-4} ^b	0.9 ^r	−2.9702	0.29669	3.0866	9.07	8.68×10^{33}	4.0×10^{32} [★]
LMC X-1 [†]	10.91 ^s	0.884 ^t	0.92 ^t	−4.1158	0.26757	3.9125	8.972	4.71×10^{37}	2.0×10^{39} ^u
Cyg X-1 [†]	14.8 ^v	0.061 ^w	0.97 ^x	−3.3274	0.35534	3.4323	8.02	3.87×10^{36}	1.0×10^{37} ^y
GRS1915+105 [†]	10.1 ^z	3.188 ^{zx}	0.98 ^{zy}	−3.5997	0.36401	3.4312	8.02	1.38×10^{38}	1.0×10^{38} ^{zx}

In Column (1), we make a list of the names of the sources and in Cols. (2)–(4) we give the corresponding mass, accretion rate and spin. In Cols. (5)–(6), we report the model parameters and in Cols. (7)–(9), we indicate the maximum energy dissipated, the shock location and the estimated maximum luminosity of shock obtained using Eq. (15). The core radio luminosity values reported from observations are listed in Col. (10).

^aCantrell et al. (2010); ^bYang (2016); ^cGou et al. (2010); ^dOrosz et al. (2014); ^eKubota et al. (2010); ^fSteiner et al. (2014); ^gMolla et al. (2017); ^hBhattacharjee et al. (2017); ⁱTursunov & Kološ (2018); ^jOrosz et al. (2011b); ^kSteiner et al. (2011); ^lFender et al. (2004); ^mMotta et al. (2014); ⁿLuketic et al. (2010); ^oShafee et al. (2006); ^pMigliari et al. (2007); ^qKhargharia et al. (2013); ^rChaty et al. (2003); ^sOrosz et al. (2009); ^tGou et al. (2009); ^uCooke et al. (2007); ^vOrosz et al. (2011a); ^wGou et al. (2011); ^xFabian et al. (2012); ^yGallo et al. (2005); ^zSteehgs et al. (2013); ^{zx}Belloni et al. (2000); ^{zy}Miller et al. (2013).

[★] $L_{\text{jet}}^{\text{Obs}} = \dot{M}_{\text{out}}c^2$ is applied for the sources A0620–00, XTE J1118+480 and H1743–322, where \dot{M}_{out} is the outflow rate. For the sources A0620–00 and XTE J1118+480, the outflow rate is adopted from Yang (2016). For H1743–322, \dot{M}_{out} is considered following Miller et al. (2006).

umn 10) reported from observations (Fender et al. 2004; Cooke et al. 2007; Gallo et al. 2007; Migliari et al. 2007; Belloni et al. 2000), subject to availability. To estimate the observed jet luminosity ($L_{\text{jet}}^{\text{Obs}}$) from the outflow rate (\dot{M}_{out}), we have employed the relation $L_{\text{jet}}^{\text{Obs}} = \dot{M}_{\text{out}}c^2$. Here, we assume 100% energy conversion efficiency on the basis of the common definition $L_{\text{Edd}} = \dot{M}_{\text{Edd}}c^2$ for the Eddington limit on the mass accretion rate adopted by many authors (Rezzolla & Zanotti 2013; Straub et al. 2014; Yuan & Narayan 2014). Although 100% energy conversion efficiency is unphysical, the definition used would give us the maximum observed luminosity achievable from the outflow rate available in the literature, which is compared with the calculated maximum shock luminosity from our model. For the BH sources marked with superscript †, the reported values of spin from the literature exceed 0.8. In such a case, it is inappropriate to apply the Chakrabarti & Mondal (2006) potential to calculate the shock luminosity corresponding to these sources. Nevertheless, we carry out the analysis using this potential in order to get a qualitative estimate of $\mathcal{L}_{\text{shock}}^{\text{max}}$ for these sources.

5 SUMMARY

We study the effects of the variation of magnetic flux advection rate ($\dot{\Phi}$) and accretion rate (\dot{m}) on the properties of shock in accretion flow around a rapidly rotating BH ($a_s = 0.8$). In the global transonic accretion solutions, heating takes place due to the thermalization of magnetic energy, while cooling occurs via synchrotron emission. In Figure 1, we present the combined effect of variation of \dot{m} and ζ -parameter on the shock dynamics. For fixed injec-

tion parameters at the outer edge, we find that the shock location shifts towards the horizon with the increase of ζ (via the corresponding increase of $\dot{\Phi}$) as well as the increase of \dot{m} . In Figure 2, we have demonstrated the radial variation of various flow variables corresponding to the global shocked accretion solutions considered in Figure 1. We observe that the PSC is hotter, denser, optically thick and also contains higher magnetic field strength as compared to the pre-shock flow. In Figure 3, we examine the effect of the increase of ζ on the shock dynamics. The increase of ζ leads to the increase of toroidal magnetic flux advection rate in the radial direction as the flow gets closer to the BH. With the increase of magnetic activity in the disc, the flow is efficiently cooled. Since the cooling efficiency is greater in the PSC due to higher temperature and density there, the post-shock pressure drops and the shock front is pushed towards the BH in order to maintain pressure balance across it. The increase of magnetic activity in the disc (due to increase of ζ) also enhances the angular momentum transport towards the outer region of the disc. This further weakens the centrifugal repulsion against gravity and also contributes to shift the shock towards the horizon. As a consequence, the shock compression ratio (R) and the shock strength (Θ) also rise (Figs. 3(b) and 3(c)). Furthermore, from Figure 3 we also observe that global accretion solutions with shock exist for an ample range of ζ -parameter and angular momentum. Next in Figure 4, we explore the effect of increase of \dot{m} on the shock position. For a given set of injection parameters at the outer edge, we observe that global shocked accretion solutions exist for a wide range of \dot{m} . However, the range of \dot{m} for shock

anti-correlates with the increase of ζ . Finally in Section 4, we consider the astrophysical application of the present formalism. We estimate the maximum energy dissipated across the shock front via the thermal Comptonization phenomenon and the corresponding shock luminosity ($\mathcal{L}_{\text{shock}}^{\text{max}}$) for several stellar mass BHCs. We find that the estimated $\mathcal{L}_{\text{shock}}^{\text{max}}$ is in good agreement with the observed values of jet kinetic luminosity ($\mathcal{L}_{\text{jet}}^{\text{Obs}}$). If the value of $\mathcal{L}_{\text{jet}}^{\text{Obs}}$ is unavailable for a given source, the present model can predict the maximum shock luminosity $\mathcal{L}_{\text{shock}}^{\text{max}}$ that may be observed.

In the end, we would like to mention the limitations of the present formalism. For the sake of simplicity, we have adopted the Chakrabarti & Mondal (2006) pseudo-Kerr potential to mimic the general relativistic effects around a rotating BH. The potential gives satisfactory results till spin value $a_s \leq 0.8$. Thus, the accretion flow properties around an extremely rapidly rotating BH cannot be explored satisfactorily in the present approach. Although we have attempted to calculate $\mathcal{L}_{\text{max}}^{\text{shock}}$ for four stellar mass BHCs with $a_s > 0.8$, this provides only a qualitative estimate. Again, the magnetic fields are likely to cause the generation of jets and outflows from the disc, which have not been considered in the present work. Moreover, the adiabatic index is considered to be a global constant in the paper, although it should be calculated self-consistently from the global accretion solution. Since the magnetized accretion flow in this work remains optically thin throughout (Fig. 2(f)), Comptonization of the soft synchrotron photons that are produced locally would be important (Yuan & Narayan 2014). However, to carry out a simplistic treatment, we have excluded the cooling effect due to Comptonization in this work. Ipser & Price (1983) have indicated that the radiative cooling efficiency in the accretion flow is enhanced due to the Comptonization process. Again, recently Dihingia et al. (2018b) examined two-temperature shocked accretion flows around BHs including the effect of Comptonization. In this work, the authors demonstrated that due to the rise in density of the PSC as a result of shock transition, all the radiative processes in the flow viz, bremsstrahlung, synchrotron and Comptonization due to synchrotron photons, are very efficient in the PSC. Thus for fixed outer boundary conditions, if Comptonization due to synchrotron photons is included in our present work, we expect that the radiative cooling in the PSC would be enhanced and the shock location would shift towards the horizon in order to maintain the pressure balance across the shock. This will result in a quantitative change in the related shock properties as reported in the present work. For example, the shock compression ratio (R), shock strength (Θ) and critical limits of ζ and \dot{m} , as depicted in Figures (3) and (4), would be quantitatively modified. However, the qualitative behavior of the results

is expected to remain unaltered. We would like to address these issues in the future.

Acknowledgements BS acknowledges Dr. Ramiz Aktar and Mr. Indu Kalpa Dihingia for useful discussions on specific topics of the paper. AR acknowledges a Commonwealth Rutherford Fellowship. Authors would like to thank the referee for his valuable comments and constructive suggestions, which helped to improve the presentation of the paper.

References

- Abramowicz, M. A., Chen, X., Kato, S., Lasota, J.-P., & Regev, O. 1995, *ApJ*, 438, L37
- Aktar, R., Das, S., & Nandi, A. 2015, *MNRAS*, 453, 3414
- Artemova, I. V., Bjoernsson, G., & Novikov, I. D. 1996, *ApJ*, 461, 565
- Balbus, S. A., & Hawley, J. F. 1991, *ApJ*, 376, 214
- Becker, P. A., & Kazanas, D. 2001, *ApJ*, 546, 429
- Belloni, T., Migliari, S., & Fender, R. P. 2000, *A&A*, 358, L29
- Bhattacharjee, A., Banerjee, I., Banerjee, A., Debnath, D., & Chakrabarti, S. K. 2017, *MNRAS*, 466, 1372
- Blandford, R. D., & Payne, D. G. 1982, *MNRAS*, 199, 883
- Blandford, R. D., & Znajek, R. L. 1977, *MNRAS*, 179, 433
- Cantrell, A. G., Bailyn, C. D., Orosz, J. A., et al. 2010, *ApJ*, 710, 1127
- Chakrabarti, S. K. 1989, *ApJ*, 347, 365
- Chakrabarti, S. K. 1990, *Theory of Transonic Astrophysical Flows* (World Scientific Publishing Co. Pte. Ltd)
- Chakrabarti, S. K., & Khanna, R. 1992, *MNRAS*, 256, 300
- Chakrabarti, S., & Titarchuk, L. G. 1995, *ApJ*, 455, 623
- Chakrabarti, S. K., Acharyya, K., & Molteni, D. 2004, *A&A*, 421, 1
- Chakrabarti, S. K., & Das, S. 2004, *MNRAS*, 349, 649
- Chakrabarti, S. K., & Mondal, S. 2006, *MNRAS*, 369, 976
- Chattopadhyay, I., & Chakrabarti, S. K. 2002, *MNRAS*, 333, 454
- Chattopadhyay, I., & Chakrabarti, S. K. 2011, *International Journal of Modern Physics D*, 20, 1597
- Chaty, S., Haswell, C. A., Malzac, J., et al. 2003, *MNRAS*, 346, 689
- Cooke, R., Kuncic, Z., Sharp, R., & Bland -Hawthorn, J. 2007, *ApJ*, 667, L163
- Das, S., Chattopadhyay, I., Nandi, A., & Chakrabarti, S. K. 2001, *A&A*, 379, 683
- Das, S., & Choi, C.-S. 2009, *Ap&SS*, 321, 109
- Das, S., Chakrabarti, S. K., & Mondal, S. 2010, *MNRAS*, 401, 2053
- Das, S., Chattopadhyay, I., Nandi, A., & Molteni, D. 2014a, *MNRAS*, 442, 251
- Das, S., Chattopadhyay, I., Nandi, A., & Sarkar, B. 2014b, *Bulletin of the Astronomical Society of India*, 42, 39
- Das, S., & Sarkar, B. 2018, *MNRAS*, 480, 3446
- Dihingia, I. K., Das, S., Maity, D., & Chakrabarti, S. 2018a, *Phys. Rev. D*, 98, 083004

- Dihingia, I. K., Das, S., & Mandal, S. 2018b, *MNRAS*, 475, 2164
- Dihingia, I. K., Das, S., & Nandi, A. 2019, *MNRAS*, 484, 3209
- Fabian, A. C., Wilkins, D. R., Miller, J. M., et al. 2012, *MNRAS*, 424, 217
- Fender, R. P., Belloni, T. M., & Gallo, E. 2004, *MNRAS*, 355, 1105
- Frank, J., King, A., & Raine, D. 1992, *Accretion Power in Astrophysics.*, 21 (Camb. Astrophys. Ser., 21)
- Fukue, J. 1987, *PASJ*, 39, 309
- Fukumura, K., & Tsuruta, S. 2004, *ApJ*, 611, 964
- Gallo, E., Fender, R., Kaiser, C., et al. 2005, *Nature*, 436, 819
- Gallo, E., Migliari, S., Markoff, S., et al. 2007, *ApJ*, 670, 600
- Ghosh, S., & Mukhopadhyay, B. 2007, *ApJ*, 667, 367
- Ghosh, S., Sarkar, T., & Bhadra, A. 2014, *MNRAS*, 445, 4463
- Gou, L., McClintock, J. E., Liu, J., et al. 2009, *ApJ*, 701, 1076
- Gou, L., McClintock, J. E., Steiner, J. F., et al. 2010, *ApJ*, 718, L122
- Gou, L., McClintock, J. E., Reid, M. J., et al. 2011, *ApJ*, 742, 85
- Gu, W.-M., & Lu, J.-F. 2004, *Chinese Physics Letters*, 21, 2551
- Hirose, S., Krolik, J. H., & Stone, J. M. 2006, *ApJ*, 640, 901
- Ichimaru, S. 1977, *ApJ*, 214, 840
- Ipsier, J. R., & Price, R. H. 1983, *ApJ*, 267, 371
- Ivanov, R. I., & Prodanov, E. M. 2005, *Physics Letters B*, 611, 34
- Johansen, A., & Levin, Y. 2008, *A&A*, 490, 501
- Karas, V., & Abramowicz, M. A. 2014, in *Proceedings of RAGtime 10–13: Workshops on Black Holes and Neutron Stars*, 121
- Khargharia, J., Froning, C. S., Robinson, E. L., & Gelino, D. M. 2013, *AJ*, 145, 21
- Krolik, J. H., Hirose, S., & Blaes, O. 2007, *ApJ*, 664, 1045
- Kubota, A., Done, C., Davis, S. W., et al. 2010, *ApJ*, 714, 860
- Kumar, R., & Chattopadhyay, I. 2013, *MNRAS*, 430, 386
- Landau, L. D., & Lifshitz, E. M. 1959, *Fluid Mechanics (Course of Theoretical Physics, Oxford: Pergamon Press)*
- Le, T., & Becker, P. A. 2004, *ApJ*, 617, L25
- Le, T., & Becker, P. A. 2005, *ApJ*, 632, 476
- Løvås, T. 1998, *International Journal of Modern Physics D*, 7, 471
- Lu, J.-F., & Yuan, F. 1998, *MNRAS*, 295, 66
- Luketic, S., Proga, D., Kallman, T. R., Raymond, J. C., & Miller, J. M. 2010, *ApJ*, 719, 515
- Machida, M., Nakamura, K. E., & Matsumoto, R. 2006, *PASJ*, 58, 193
- Mahadevan, R., & Quataert, E. 1997, *ApJ*, 490, 605
- Matsumoto, R., Kato, S., Fukue, J., & Okazaki, A. T. 1984, *PASJ*, 36, 71
- Migliari, S., Tomsick, J. A., Markoff, S., et al. 2007, *ApJ*, 670, 610
- Miller, J. M., Raymond, J., Homan, J., et al. 2006, *ApJ*, 646, 394
- Miller, J. M., Parker, M. L., Fuerst, F., et al. 2013, *ApJ*, 775, L45
- Molla, A. A., Chakrabarti, S. K., Debnath, D., & Mondal, S. 2017, *ApJ*, 834, 88
- Molteni, D., Sponholz, H., & Chakrabarti, S. K. 1996, *ApJ*, 457, 805
- Mondal, S., Chakrabarti, S. K., & Debnath, D. 2014, *Ap&SS*, 353, 223
- Motta, S. E., Belloni, T. M., Stella, L., Muñoz-Darias, T., & Fender, R. 2014, *MNRAS*, 437, 2554
- Mukhopadhyay, B. 2002, *ApJ*, 581, 427
- Narayan, R., & Yi, I. 1994, *ApJ*, 428, L13
- Narayan, R., & Yi, I. 1995, *ApJ*, 452, 710
- Oda, H., Machida, M., Nakamura, K. E., & Matsumoto, R. 2007, *PASJ*, 59, 457
- Oda, H., Machida, M., Nakamura, K. E., & Matsumoto, R. 2010, *ApJ*, 712, 639
- Oda, H., Machida, M., Nakamura, K. E., Matsumoto, R., & Narayan, R. 2012, *PASJ*, 64, 15
- Orosz, J. A., Steeghs, D., McClintock, J. E., et al. 2009, *ApJ*, 697, 573
- Orosz, J. A., McClintock, J. E., Aufdenberg, J. P., et al. 2011a, *ApJ*, 742, 84
- Orosz, J. A., Steiner, J. F., McClintock, J. E., et al. 2011b, *ApJ*, 730, 75
- Orosz, J. A., Steiner, J. F., McClintock, J. E., et al. 2014, *ApJ*, 794, 154
- Rajesh, S. R., & Mukhopadhyay, B. 2010, *MNRAS*, 402, 961
- Rezzolla, L., & Zanotti, O. 2013, *Relativistic Hydrodynamics (Oxford Univ. Press)*
- Sarkar, B., & Das, S. 2013, in *Astronomical Society of India Conference Series*, 8, 143
- Sarkar, B., & Das, S. 2015, in *Astronomical Society of India Conference Series*, 12, 91
- Sarkar, B., & Das, S. 2016, *MNRAS*, 461, 190
- Sarkar, B., & Das, S. 2018, *Journal of Astrophysics and Astronomy*, 39, 3
- Sarkar, B., Das, S., & Mandal, S. 2018, *MNRAS*, 473, 2415
- Semerák, O., & Karas, V. 1999, *A&A*, 343, 325
- Shafee, R., McClintock, J. E., Narayan, R., et al. 2006, *ApJ*, 636, L113
- Shakura, N. I., & Sunyaev, R. A. 1973, *A&A*, 500, 33
- Shapiro, S. L., & Teukolsky, S. A. 1983, *Black Holes, White Dwarfs, and Neutron Stars : the Physics of Compact Objects (New York: A Wiley-Interscience Publication)*
- Singh, C. B., & Chakrabarti, S. K. 2011, *MNRAS*, 410, 2414
- Steeghs, D., McClintock, J. E., Parsons, S. G., et al. 2013, *ApJ*, 768, 185
- Steiner, J. F., Reis, R. C., McClintock, J. E., et al. 2011, *MNRAS*, 416, 941
- Steiner, J. F., McClintock, J. E., Orosz, J. A., et al. 2014, *ApJ*, 793, L29
- Straub, O., Godet, O., Webb, N., Servillat, M., & Barret, D. 2014, *A&A*, 569, A116
- Tursunov, A. A., & Kološ, M. 2018, *Physics of Atomic Nuclei*, 81, 279
- Yang, Q.-X. 2016, *RAA (Research in Astronomy and Astrophysics)*, 16, 62
- Yuan, F., & Narayan, R. 2014, *ARA&A*, 52, 529